

Effect of Calcium Ions and CaCO₃ Scale on the CO₂ Corrosion Mechanism of Mild Steel

Hamed Mansoori, Bruce Brown, David Young, Srdjan Nestic, Marc Singer
Institute for Corrosion and Multiphase Technology,
Department of Chemical & Biomolecular Engineering, Ohio University
342 West State Street
Athens, OH, 45701
USA

ABSTRACT

Calcium ions are usually present at high concentrations in brines produced with oil and gas. Such brines are often saturated with respect to calcium carbonate (CaCO₃). Consequently, precipitation of CaCO₃ as scale on the internal wall of the pipeline can readily occur due to changes in operational and environmental parameters as produced fluids are transferred from downhole to surface facilities. Despite its importance, there is minimal research in the literature addressing the effect of calcium ions, and specifically CaCO₃ scale, on the CO₂ corrosion mechanism. The main objectives of this research are to further broaden the mechanistic understanding of CO₂ corrosion of mild steel in the presence of high concentrations of calcium ions and evaluate the protectiveness of CaCO₃ scale against further corrosion. The corrosion behavior was studied *in situ* by electrochemical methods, including linear polarization resistance (LPR) and open circuit potential (OCP) measurements, along with weight loss (WL), using a UNS G10180 steel with ferritic-pearlitic microstructure. Surface characterization of the scale and corrosion product was performed using scanning electron microscopy (SEM), energy dispersive X-ray spectroscopy (EDS), and X-ray diffraction (XRD). A descriptive model is proposed for the CO₂ corrosion mechanism of mild steel in the presence of high concentrations of calcium ions. Unprotective CaCO₃ scale was observed to act as a mass transfer barrier that promotes development of surface conditions favoring FeCO₃ precipitation. The presence of CaCO₃ scale did not result in onset of localized corrosion in the current experimental conditions.

Key words: *CO₂ Corrosion; Corrosion Mechanism; Mild Steel; FeCO₃; CaCO₃ Scale; Calcium Ion*

INTRODUCTION

Over the past decades, mechanisms of CO₂ corrosion of mild steel and the characteristics of its corrosion products have been intensively studied and documented by different researchers¹⁻⁶. However, most of these studies have been performed in various dilute solutions of sodium chloride (NaCl), while,

in reality, calcium ions are also present in brines associated with geologic formations⁷⁻¹⁰. CaCO_3 (mineralogical name: calcite) and FeCO_3 (siderite) are isostructural with a hexagonal unit cell. This indicates that their constituent cations (Ca^{2+} and Fe^{2+}) can coexist in a substitutional mixed carbonate, designated with the formula $\text{Fe}_x\text{Ca}_y\text{CO}_3$ (where $x+y=1$)¹¹. The solubility of CaCO_3 in water is about two orders of magnitude greater than the solubility of FeCO_3 . Therefore, substitution of Fe^{2+} by Ca^{2+} in the lattice of FeCO_3 can be hypothesized to alter the solubility of the mixed carbonate layers in comparison with pure FeCO_3 layers. In addition, compositional heterogeneity and morphological alteration are expected when Ca^{2+} incorporates into the FeCO_3 crystal structure. This suggests that the presence of Ca^{2+} in the solution and possible precipitation of CaCO_3 scale on the steel surface would influence the CO_2 corrosion mechanism.

There are only a handful of studies in the literature that address the effect of Ca^{2+} and/or CaCO_3 scale on CO_2 corrosion¹²⁻¹⁴. Such studies rely on the initial Ca^{2+} concentration rather than on the CaCO_3 saturation degree of the bulk solution as the core influential parameter. In addition, the flow characteristics of the experimental setups are often not well-defined, rendering the results difficult to reproduce¹¹. When a solution is initially supersaturated with respect to CaCO_3 , precipitation of CaCO_3 is inevitable due to its fast kinetics; particularly at elevated temperatures. Once precipitation has started, the solution tends to reach an equilibrium state with a saturation with respect to CaCO_3 approaching unity. This can lead to significant changes in water chemistry (different pH, $[\text{Ca}^{2+}]$, etc.) from the initial conditions (before precipitation) to the final conditions (after precipitation). That is why the results of such studies, which are nominally similar, often appear contradictory due to the uncontrolled changes in water chemistry and the poorly controlled flow conditions. These discrepancies necessitate the development of a systematic and well-designed procedure for elucidating the relevant issues surrounding CO_2 corrosion in the presence of Ca^{2+} and/or CaCO_3 scale. Two main environmental conditions have been identified as relevant corrosion scenarios in oilfield pipelines conditions:

- 1- A brine saturated with respect to CaCO_3 . This scenario can involve various Ca^{2+} concentrations corresponding to the pH and temperature of the solution, CO_2 partial pressure, etc.
- 2- An initially super-saturated brine leading to quick precipitation of a CaCO_3 scale on a steel surface after which the brine remains close to saturated with respect to CaCO_3 .

Tavares, *et al.*, performed one of the rare CO_2 corrosion studies on carbon steel where the solution was saturated with respect to CaCO_3 over the course of experiments, achieved by adding bulk CaCO_3 to the test solution, in accordance with the 1st scenario¹⁵. The authors reported that general corrosion was predominant rather than pitting corrosion. Moreover, they observed a decline in the corrosion rate over time (28 days) as determined by weight loss methods. The authors also reported that the average corrosion rate for mild steel in the CaCO_3 -saturated solution was lower than when the solution was without dissolved CaCO_3 . In fact, this could be due to a different initial pH of the two solutions rather than a direct effect of Ca^{2+} ions on surface layer protectiveness against corrosion. Mansoori, *et al.*, have recently investigated the 1st scenario in conditions where the water chemistry (e.g., pH & Fe^{2+} concentration) of the test solutions was tightly controlled over the course of long-term experiments and the mass transfer conditions of the experimental setup was well-defined¹⁶. They reported that in a CaCO_3 -saturated solution ($[\text{Ca}^{2+}] \sim 160$ ppm, $[\text{Fe}^{2+}] \sim 10$ ppm, pH 6.2, solution ionic strength 0.18M), a mixed iron-calcium carbonate, with a mole fraction of iron higher than that of calcium, formed on the steel surface. It was concluded that such an iron-calcium carbonate was as protective as pure FeCO_3 . Since the corrosion behavior of mild steel in the presence of Ca^{2+} highly depends on the characteristics of the surface layers, there is a further need to investigate the 1st scenario in harsher conditions seen in oilfield brines, for example, at higher calcium concentrations, higher ionic strength, and lower pH.

There are a handful of available research in conjunction with the 2nd scenario^{3,12,14}. For example, Esmaeely *et al.*, conducted experiments while the solution was initially supersaturated with respect to CaCO_3 (the source of Ca^{2+} was CaCl_2 salt)¹². They reported pitting corrosion attacks on mild steel in the presence of 10,000 ppm Ca^{2+} . However, the real cause and the mechanism of the observed localized corrosion remained ambiguous. Indeed, the immediately precipitated CaCO_3 scale on the steel surface was poorly characterized.

The main objectives of the current research are to further broaden the mechanistic understanding of CO₂ corrosion of mild steel in the presence of high concentrations of Ca²⁺. This is achieved by evaluating:

- Protectiveness of mixed iron/calcium carbonate layers obtained while the test solution is saturated with respect to CaCO₃ (1st scenario),
- Protectiveness of “pure” CaCO₃ scale formed in simulated CaCO₃ supersaturated conditions, while avoiding FeCO₃ precipitation (initial step towards the investigation of the 2nd scenario).

The 2nd scenario involves the investigation of the corrosion behavior of steel in conditions where high supersaturation of CaCO₃ is temporarily achieved, leading to a high rate of CaCO₃ precipitation and possibly altering the protectiveness of already formed FeCO₃. This scenario, which is one of the ultimate goals of the authors’ research work, was not directly investigated in the current study. Instead, an initial but crucial experiment was performed concerning the characterization of the protectiveness of the “pure” CaCO₃ layer itself. This step had never been done before since it is difficult to promote CaCO₃ precipitation while, at the same time, suppressing FeCO₃ formation. However, while the properties of “pure” FeCO₃ layers have been extensively investigated, this is not the case for “pure” CaCO₃.

To the authors’ best knowledge, experimental data related to the 2nd scenario are missing in the literature related to internal pipeline corrosion. However, there has been research in the context of external corrosion of buried pipelines, under cathodic protection, where CaCO₃ precipitated on the steel from soils rich with calcium ions. For example, Ghanbari, *et al.*, conducted electrochemical experiments to evaluate the effect of CaCO₃ scale formation on alternating current (AC) induced corrosion rates of X65 carbon steel at atmospheric pressure (open air) and room temperature¹⁷. They concluded that CaCO₃ deposits did not have any effect on AC corrosion rates other than by decreasing the exposed surface area of the steel. The experimental conditions of these tests were designed to add more understanding to the influence of external AC corrosion of a carbon steel pipeline under cathodic protection and in CaCO₃ scaling conditions. With so few references available that address the influence of CaCO₃ scale on CO₂ corrosion mechanisms, a gap in the knowledge related to the internal corrosion of oil and gas pipelines has been identified.

EXPERIMENTAL SETUP

Figure 1 depicts the 4-liter experimental setup employed to conduct the corrosion study described in the present paper. This apparatus is equipped with an impeller to create uniform mass transfer and uniform wall shear stress across the specimen surfaces. It includes stationary specimen holders with seals to eliminate oxygen contamination of the experimental setup during specimen retrieval from the test solution for surface analysis, as illustrated in Figure 1. In this setup, all corrosion specimens (for weight loss, surface analysis, and electrochemical measurements) experience identical flow characteristics (mass transfer rate and shear stress). The specimens are identical in size and are held in place by specimen holders located at the same radial distance from the center of the glass cell. The flow characteristics of this experimental setup have been reported in a recent publication by the authors¹⁶.

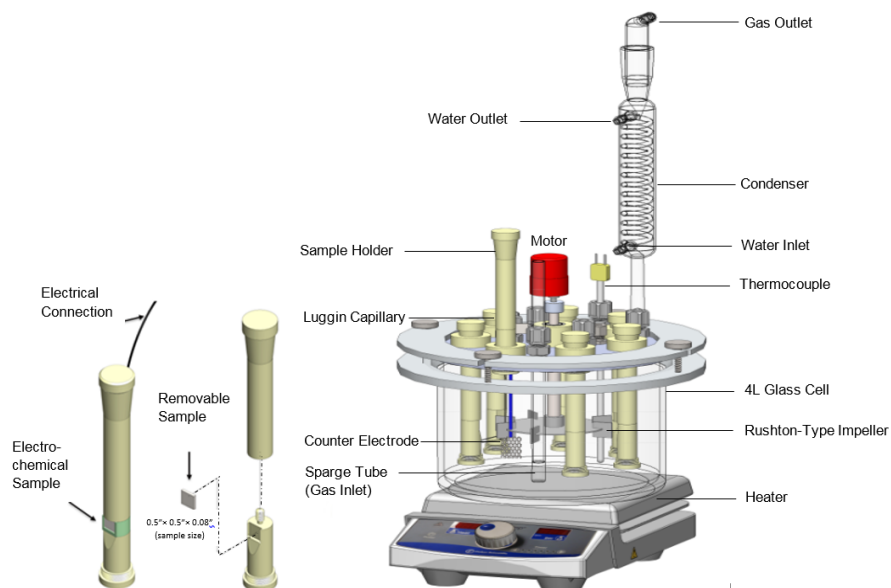


Figure 1. Schematic of experimental setup equipped with impeller, capable of ensuring uniform mass transfer across specimen surfaces and with removable specimen holders.

METHODOLOGY

To investigate the effect of high concentrations of Ca^{2+} on CO_2 corrosion (1st scenario), two series of experiments were conducted (and repeated), one in CaCO_3 -saturated solution (with $[\text{Ca}^{2+}] \sim 6000$ ppm) and one without Ca^{2+} (baseline experiment); other than that, both test series were conducted under the same conditions based on the test matrix presented in Table 1. The solutions, with and without Ca^{2+} , contained 1 wt.% NaCl in the presence of 0.53 bar pCO_2 at 80°C (1 bar total pressure of the glass cell). An excess amount of powdered CaCO_3 reagent (15 g/L) was added to the solution in order to keep it saturated with respect to CaCO_3 over the course of the 7-day experiments. This provided a $[\text{Ca}^{2+}]$ of ~ 6000 ppm in the experimental conditions. After adding CaCO_3 , the pH was adjusted with 1M HCl to a value of 5.50. For the tests without CaCO_3 , the pH was adjusted to 5.50 by adding NaHCO_3 to the solution. For the experiments without the presence of Ca^{2+} , sodium perchlorate (NaClO_4) was used to achieve the same ionic strength as in the experiments with the presence of Ca^{2+} (the ionic strength for the two experiments was 0.6M). The solutions were deoxygenated by sparging with CO_2 for two hours prior to insertion of the specimens. In addition, CO_2 was continuously bubbled into solution to maintain CO_2 saturation during corrosion experiments. The electrochemical and weight loss specimens were polished with silicon carbide abrasive papers up to 600 grit and rinsed with isopropanol. The square-shape specimens had an exposed surface area of 1.5 cm^2 . Following the polishing process, the specimens were rinsed with isopropanol and placed in an ultrasonic cleaner for 2 minutes. Finally, they were dried by cold air and immersed.

A three-electrode system (working, counter, and reference electrodes) and a Gamry[†] Reference 600[™] potentiostat were used to conduct electrochemical measurements. A platinum-coated titanium mesh with a dimension of $20 \times 30 \times 1$ mm was used as a counter electrode and saturated Ag/AgCl was used as the reference electrode. Ferrous iron (Fe^{2+}) concentration was measured twice daily by spectrophotometry using phenanthroline as the reagent¹⁸. The rotational speed of the impeller was set at 20 rpm, which provided a mass transfer rate similar to a flow velocity of 0.5 m/s in a 0.1m ID single flow pipe. The corrosion rate was measured at least twice per day using LPR, and OCP was also recorded. Solution resistance, used for adjusting the actual polarization resistance of the working electrode, was obtained by the electrochemical impedance spectroscopy (EIS) technique after each LPR reading. Two specimens were retrieved from the glass cell at days 2, 4, and 7 from each experiment to obtain weight loss and conduct surface characterization using SEM/EDS and XRD.

[†] Trade Name

Table 1. Experimental conditions to evaluate the effect of CaCO₃-saturated solutions on CO₂ corrosion in presence of high concentrations of Ca²⁺

Parameter	Description	
	without CaCO ₃	with CaCO ₃
Specimen steel	UNS G10180 with Ferritic-Pearlitic Structure Flat Square Specimen (A = 1.5 cm ²)	
Temperature	80°C	
pCO ₂	0.53 bar	
pH	5.5 ± 0.2 (adjusted by NaHCO ₃)	5.5 ± 0.1 (adjusted by HCl)
Electrolyte	1 wt.% NaCl +NaHCO ₃ +NaClO ₄ (ionic strength= 0.6 M)	1 wt.% NaCl +HCl+CaCO ₃ (ionic strength=0.6 M)
CaCO ₃ saturation degree (<i>S</i> _{CaCO₃})	0	Unity ([Ca ²⁺] _{~6000 ppm})
FeCO ₃ saturation degree (<i>S</i> _{FeCO₃})	0 to 1.2	0 to 10.8
Dissolved O ₂	0-5 ppb	
Reference Electrode	Saturated Ag/AgCl	
Impeller rotation speed	20 rpm	
Mass Transfer Conditions	Equivalent to 0.5 m/s in a 0.1m ID pipe	
Electrochemical Techniques	OCP, LPR, EIS	
Surface Analysis Techniques	XRD, SEM/EDS	
Experiment Duration	7 days	

To study the protectiveness of CaCO₃ scale (in conjunction with the 2nd scenario), a novel methodology was used. The idea was to form an artificial CaCO₃ scale, without the participation of Fe²⁺ (coming from the corroding steel) in the carbonate formation process, on the steel surface and then to evaluate its protectiveness against further corrosion. To reach this goal, two working electrodes were cathodically polarized (-200 mV versus OCP) for five days.

Table 2 shows the experimental conditions used for this series of experiments. The corrosion rate was reduced significantly by cathodic polarization, thereby minimizing Fe²⁺ production (the Fe²⁺ concentration was so low that it was not detectable in the bulk solution by spectrophotometry). The bulk solution was kept saturated with respect to CaCO₃ by introducing an excess amount of powdered CaCO₃ to the solution at the beginning of the experiments (providing ~6000 ppm dissolved Ca²⁺). The experimental conditions used for this series of experiments were identical to those for the 1st scenario corrosion experiments except that here the specimens were cathodically protected in order to form pure CaCO₃ scale on the steel surface, while suppressing any Fe²⁺ release by corrosion and any formation of FeCO₃. During cathodic protection, the surface pH of the specimen was much higher than the bulk solution due to the acceleration of hydrogen evolution reactions and consumption of hydrogen ions. Therefore, the surface water chemistry was favorable for precipitation of CaCO₃ scale in the absence of Fe²⁺. LPR and OCP measurements were performed once a day when the cathodic polarization was temporarily removed (for approximately 5 minutes) in order to observe the effect of CaCO₃ scale formation on corrosion rate. After 5 days, the cathodic protection was stopped and one specimen was retrieved from the test solution for surface characterization while the other specimen (now covered with CaCO₃ scale) continued to be exposed to the corrosive solution that was saturated with CaCO₃.

Table 2. Experimental conditions employed to evaluate protectiveness of CaCO₃ scale

Temperature	80°C
pCO ₂	0.53 bar
pH	5.50 ± 0.1
Electrolyte	1 wt.% NaCl+HCl+CaCO ₃ (ionic strength=0.6 M)
CaCO ₃ saturation degree in bulk solution	Unity (~6000 ppm Ca ²⁺)
Impeller rotation speed	20 rpm
Mass transfer conditions	Equivalent to 0.5 m/s in a 0.1m ID pipe
Specimen steel	UNS G10180
Cathodic polarization potential	-200 mV vs. OCP
Methods for monitoring corrosion behavior	LPR, OCP
Cathodic protection duration (formation of CaCO ₃)	5 days
Pre-scaled (CaCO ₃) specimen exposed for active corrosion	7 days

EXPERIMENTAL RESULTS

Effect of High Concentrations of Ca²⁺ (1st scenario: Mixed iron-calcium carbonate)

Within this research, a special effort was made to maintain comparable water chemistry in all experiments listed in the test matrix presented in Table 1. Figure 2 shows the bulk solution pH for experiments with and without Ca²⁺ over time. Solution pH was maintained at pH 5.5 by adding hydrochloric acid (HCl) when it was necessary during the experiment without the presence of Ca²⁺. The CaCO₃-saturated solution showed a strong buffering capacity over the course of experiments, therefore, the solution pH was “self-controlled” at its initial value of pH 5.5. Such buffering behavior was also reported by Duan, *et al.* ²⁴. FeCO₃ saturation degree (S_{FeCO_3}) is an import parameter in CO₂ corrosion studies, influencing precipitation rate of FeCO₃ and thus the corrosion behavior ²⁵. Figure 3 compares the FeCO₃ saturation degree of the bulk solution for experiments with and without Ca²⁺ over time. S_{FeCO_3} was calculated using Equation (4):

$$S_{FeCO_3} = \frac{C_{Fe^{2+}} * C_{CO_3^{2-}}}{K_{sp,FeCO_3}} \quad (4)$$

where $C_{Fe^{2+}}$ and $C_{CO_3^{2-}}$ are ferrous ion (Fe²⁺) and carbonate ion (CO₃²⁻) concentrations in the bulk solution. Fe²⁺ was measured and CO₃²⁻ was calculated based on the measured pH and using an equilibrium model for CO₂ speciation in aqueous environments ²⁶. The $K_{sp,FeCO_3}$ in Equation (4) is the solubility product of FeCO₃ calculated using an equation proposed by Sun, *et al.* ²⁷:

$$\log K_{SP,FeCO_3} = -59.3498 - 0.041377 * T_k - \frac{2.1963}{T_k} + 24.5724 * \text{Log}(T_k) + 2.518 * I^{0.5} - 0.657 * I \quad (5)$$

where T_k is the temperature (in Kelvin) and I is the ionic strength. Fe²⁺ was introduced into the bulk solution due to the corrosion process and, as a result, FeCO₃ saturation was increased over time for experiments with and without Ca²⁺. However, the final value of FeCO₃ saturation for the experiment without Ca²⁺ was higher than the experiment with Ca²⁺ due to its higher corrosion rate and, thus, higher Fe²⁺ concentrations in the bulk. The final FeCO₃ saturation value for experiments with and without Ca²⁺ was 1.2 and 10.8, respectively (see Figure 3).

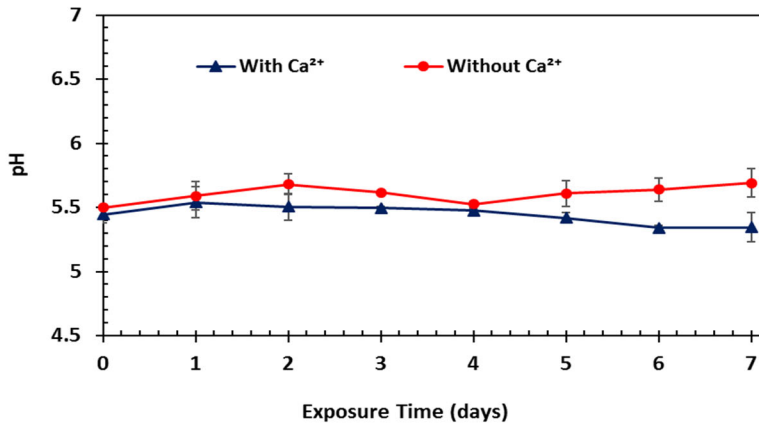


Figure 2. Variation of bulk solution pH over time for experiments with and without Ca²⁺

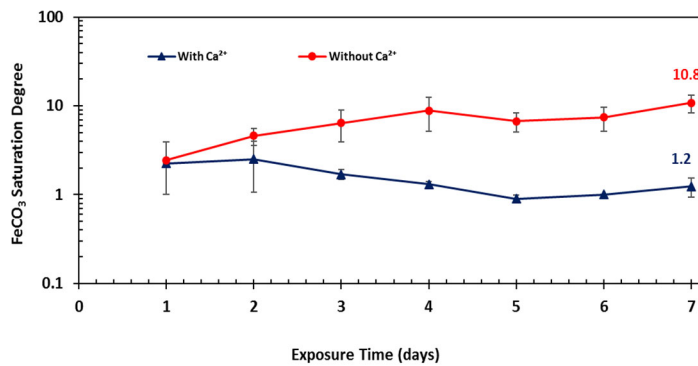


Figure 3. Variation of FeCO₃ saturation degree over time for the experiments with and without Ca²⁺

The LPR corrosion rate of the steel specimens for experiments conducted in the presence of 6000 ppm Ca²⁺ (solution was saturated with respect to CaCO₃) is compared with that of baseline conditions (in the absence of Ca²⁺ ions) in Figure 4 using a B value of 26 mV/decade. The error bars in Figure 4, and other figures throughout this paper, represent the maximum and minimum values at each data point obtained from two different experiments.

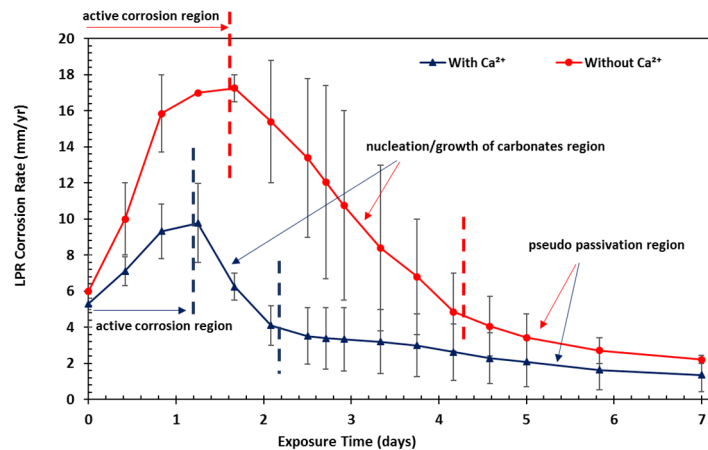


Figure 4. Comparison of LPR corrosion rates of UNS G10180 exposed to solutions with and without Ca²⁺

Three corrosion regions were identified for both experiments with and without Ca^{2+} ions based on Figure 4; 1-active corrosion, 2-nucleation and growth of carbonates, and 3-pseudo-passivation region. Within this paper, ‘pseudo-passivation’ refers to the decrease in corrosion rate observed with a simultaneous increase in corrosion potential¹⁹. A semi-conductive cementite phase (Fe_3C) has been reported as the early stage corrosion product for a UNS G10180 steel²⁰. Fe_3C is often found on the steel surface, derived from the pre-existing ferritic-pearlitic microstructure, due to the preferential dissolution of the ferrite phase ($\alpha\text{-Fe}$) over Fe_3C in the corrosion process. It has been reported that the presence of Fe_3C increases corrosion rate through a galvanic effect and provides more cathodic sites for the hydrogen evolution reaction (HER)^{21,22}. The possible pathway for hydrogen evolution reactions in CO_2 aqueous environments can be described as follows:



As can be seen from Figure 4, the active corrosion region was shorter and the LPR corrosion rate was lower in the presence of Ca^{2+} . However, for both experiments, corrosion rate dropped after reaching maximum values of 9 mm/y and 19 mm/yr for experiments with and without Ca^{2+} , respectively. Cross-sectional characterization and SEM/EDS analysis were performed on the specimens retrieved from the test solutions at the different exposure times for both series of experiments. Such investigations revealed that the drop of corrosion rate in the second region was due to nucleation and growth of carbonate layers within the Fe_3C network and adjacent to the steel surface. (Results of surface characterization will be discussed in more detail in the next section.) In the pseudo-passivation region, the corrosion rates with and without Ca^{2+} decreased. This was mainly attributed to the fact that corrosion product layers became denser and more compact during this time. It should be mentioned that the residual corrosion rate in this region was still high for experiments with and without Ca^{2+} (see Figure 4). Other researchers have also observed the same results as such a corrosion product layer could not offer a good level of protectiveness at low bulk solution pH (*i.e.*, pH 5.5)²³. However, the final corrosion rate was lower in the presence of Ca^{2+} . This indicated that the corrosion products in the presence of Ca^{2+} were more protective. Two specimens were pulled out from the test solutions at days 2, 4, and 7 of the experiments for surface layer characterizations and measuring corrosion rate by weight loss techniques. Figure 5 shows a comparison of corrosion rate by WL at different exposure times. This graph indicates that the corrosion rate by WL was approximately two times higher in the absence of Ca^{2+} . Similarly to the corrosion rates obtained by LPR, WL methods showed that the corrosion rate was decreasing over time for both series of experiments.

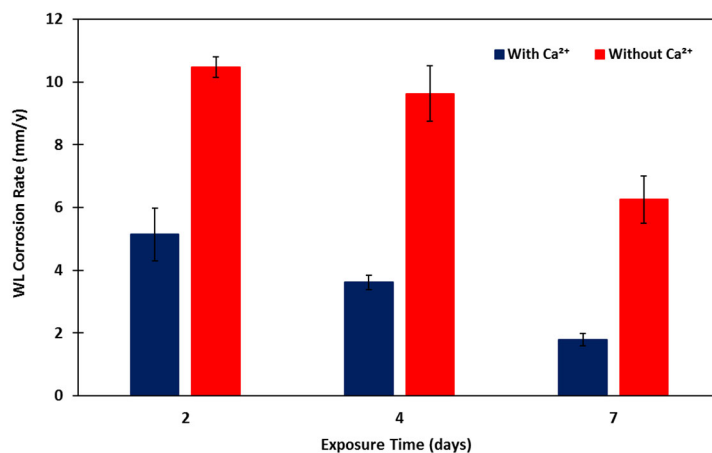


Figure 5. WL corrosion rate over time for solution with and without Ca^{2+}

A comparison of OCP in solutions with and without Ca^{2+} is shown in Figure 6. The initial OCP for both experiments was almost the same and it became more positive after the carbonate layers formed on the steel surface.

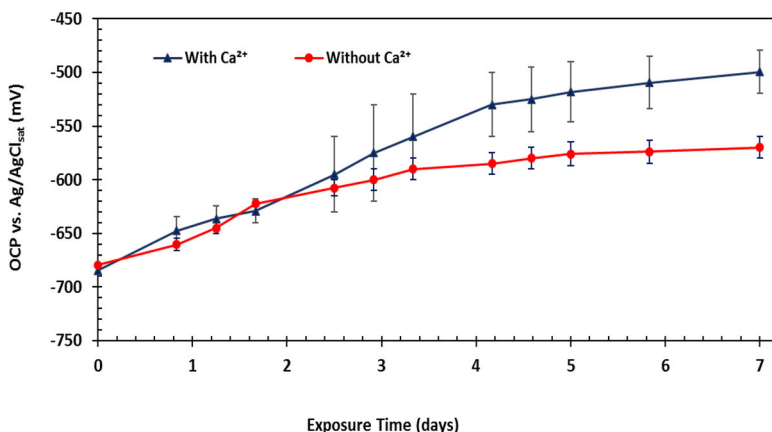


Figure 6. Comparison of OCP over time for UNS G10180 exposed to solutions with and without Ca^{2+}

Surface Layer Characterization

Surface layers were characterized using a JEOL[‡] JSM-6390LV SEM. The chemical composition of the corrosion products and scales was analyzed by an EDS detector attached to the SEM as well as by XRD using a Rigaku Ultima[§] IV diffractometer.

Experiments without Ca^{2+}

Figure 7 shows SEM cross-sectional and top view images of surface layers developed at different exposure times for experiments conducted in the absence of Ca^{2+} . The yellow arrows on the cross-sectioned specimens indicate the calculated metal loss based on WL corrosion rate. Such values were greater than the measured physical thickness of the Fe_3C layer, indicating that shear stress created by flow could have removed some of the corrosion products from the steel surface.

Top and cross-sectional images taken for the first two days of the experiment confirm development of a porous Fe_3C layer with an approximate thickness of 24 μm . Recall that Figure 4 indicates that corrosion rate at the end of the second day (active corrosion region) was at a maximum value of 19 mm/yr (which is somewhat exaggerated by the LPR measurements that cannot cope with the galvanic coupling between the Fe_3C layer and the steel surface). The cross-section image at the end of day four suggests that a second phase precipitated within the Fe_3C network, adjacent to the steel surface. This second layer was identified to be consistent with FeCO_3 by EDS analysis (Figure 8). Upon the precipitation of FeCO_3 within the Fe_3C pores, the corrosion rate decreased and so did the layer growth rate from day 4 to day 7. A scan of the top view images at different exposure times suggests that FeCO_3 crystals did not precipitate on top of the Fe_3C layer, even though FeCO_3 saturation degree for the bulk solution reached a value of 10.8 by the end of the experiment. In fact, the development of a Fe_3C network hindered mass transfer of Fe^{2+} outward from the steel surface and resulted in a much higher concentration of Fe^{2+} near the steel surface compared to the bulk solution. Indeed, the occurrence of hydrogen evolution reactions, Reactions 1 to 4, within the Fe_3C network and on the steel surface can be postulated to increase solution pH in these areas as well. Therefore, a very different water chemistry was achieved within the Fe_3C network, which favored precipitation of FeCO_3 adjacent to the steel surface

[‡] Trade Name

[§] Trade Name

(evident from the cross-section SEM images at the end of day 4 and day 7 of the experiment). To provide more proof of such a scenario, Figure 9 shows an elemental line scan of the surface layers developed after seven days of exposure that suggests precipitation of FeCO_3 adjacent to the steel surface.

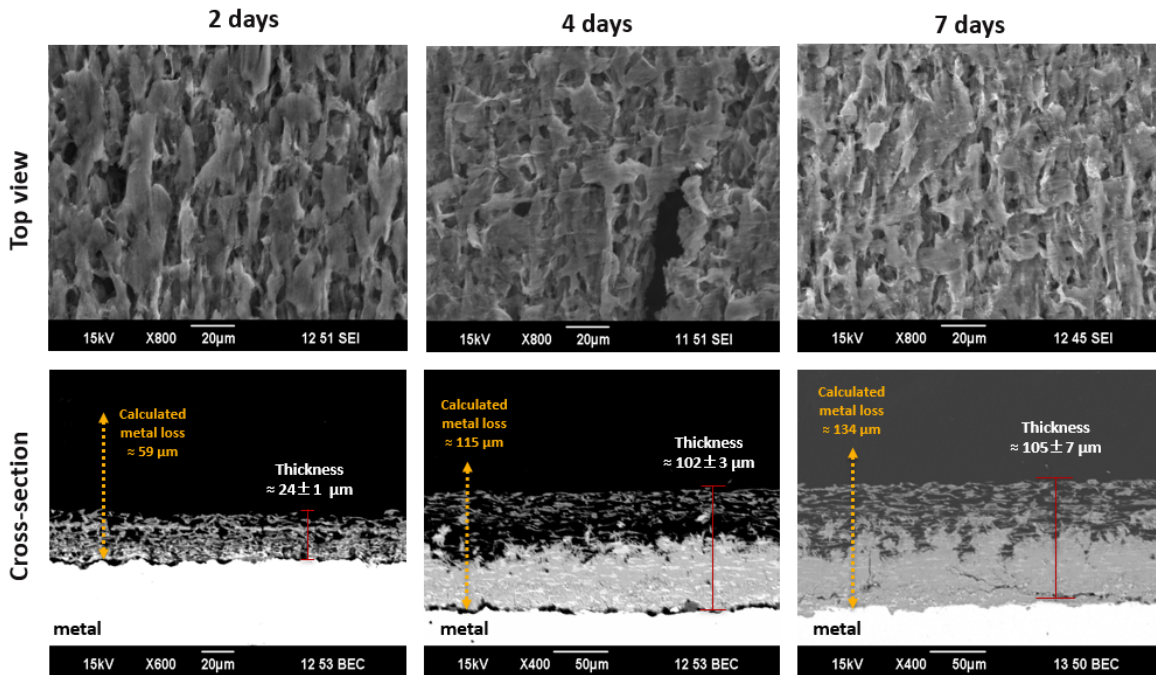


Figure 7. SEM images (top and cross-section view) of the development of surface layers over time for the experiment without Ca^{2+}

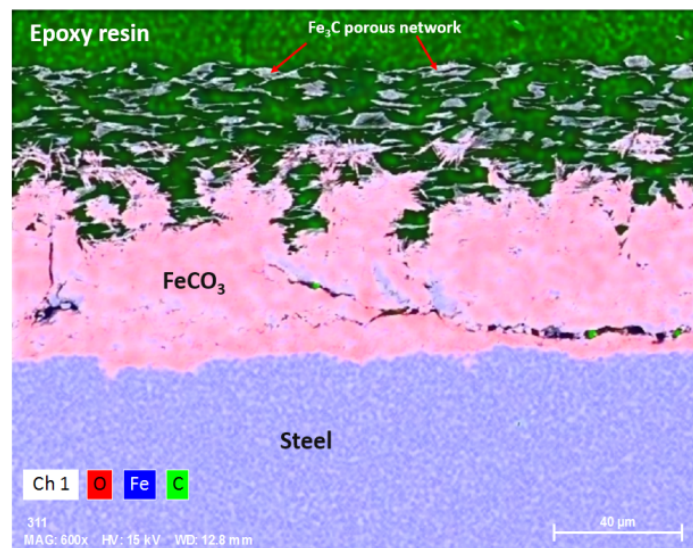


Figure 8. Cross-section SEM/EDS analysis of the corrosion products after 7 days of exposure indicating precipitation of FeCO_3 within the Fe_3C network and adjacent to the steel surface

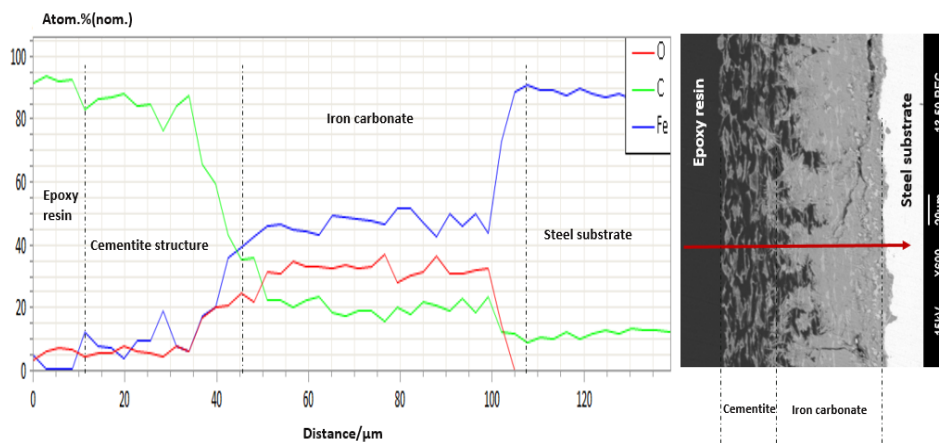


Figure 9. EDS line scan analysis of the surface layers developed after 7 days without Ca^{2+}

Experiments with 6000 ppm of Ca^{2+} (CaCO_3 saturation degree of unity)

Figure 10 shows SEM images (cross-section and top view) of surface layers developed at different exposure times for an experiment with a CaCO_3 -saturated solution. Unlike the experiment conducted in the absence of Ca^{2+} , SEM images of the top view confirmed precipitation of crystalline phases on the top of the steel surface even after two days of exposure. Such crystals did not cover the entire surface and their quantity and size grew over time (see top view images in Figure 10). EDS analysis and XRD data confirmed that such crystalline phases were substitutional iron-calcium carbonate solid solutions, with calcium being dominant over iron ($\text{Fe}_x\text{Ca}_y\text{CO}_3$, where $x+y=1$ and $x<y$). The cross-sectional SEM image of the specimen after 2 days of exposure confirmed that $\text{Fe}_x\text{Ca}_y\text{CO}_3$ was partially precipitated within the Fe_3C porous structure. Fe_3C developed as the residual, corrosion product on the steel surface. The thickness of the Fe_3C layers at this time was around $17\mu\text{m}$. A much higher pH value would have occurred within the Fe_3C pores in comparison to the pH 5.5 of the bulk solution. The bulk solution was already saturated with respect to CaCO_3 at 80°C , pH 5.5, $p\text{CO}_2$ 0.53 bar, 0.6M ionic strength, and $[\text{Ca}^{2+}] \sim 6000$ ppm. The increased pH within the Fe_3C network would favor precipitation of CaCO_3 . However, due to its presence close to the steel surface, Fe^{2+} would also be involved in the crystallization process along with Ca^{2+} and a substitutional solid solution of iron-calcium carbonate with Ca being dominant over Fe formed at this stage. Precipitation of mixed carbonates first started within the Fe_3C network, however, propagation and growth of such phases continued outside of the Fe_3C layer, which in some locations were visible from top view and cross-section images as shown in Figure 10.

Based on Figure 4, the corrosion rate was still increasing up to day 2 of the experiment without Ca^{2+} , whereas for the experiment with 6000 ppm Ca^{2+} , the corrosion rate was already decreasing well before day 2. This decrease was due to precipitation of the mixed metal carbonate within the Fe_3C matrix and as a result of partial blockage of the steel surface, retarding the anodic reaction. Cross-section morphology of the surface layers at the end of day 4 showed that almost the entire Fe_3C layer was filled with $\text{Fe}_x\text{Ca}_y\text{CO}_3$. The corrosion rate obtained by LPR showed a high value of 2.3 mm/yr at this stage (Figure 4). An immediate conclusion was that precipitation of $\text{Fe}_x\text{Ca}_y\text{CO}_3$ on the steel surface could not offer an acceptable level of protection against further corrosion, and undermining corrosion was still ongoing. That was why the thickness of surface layers grew from $35\mu\text{m}$ at day 4 to $60\mu\text{m}$ at day 7 of the experiment.

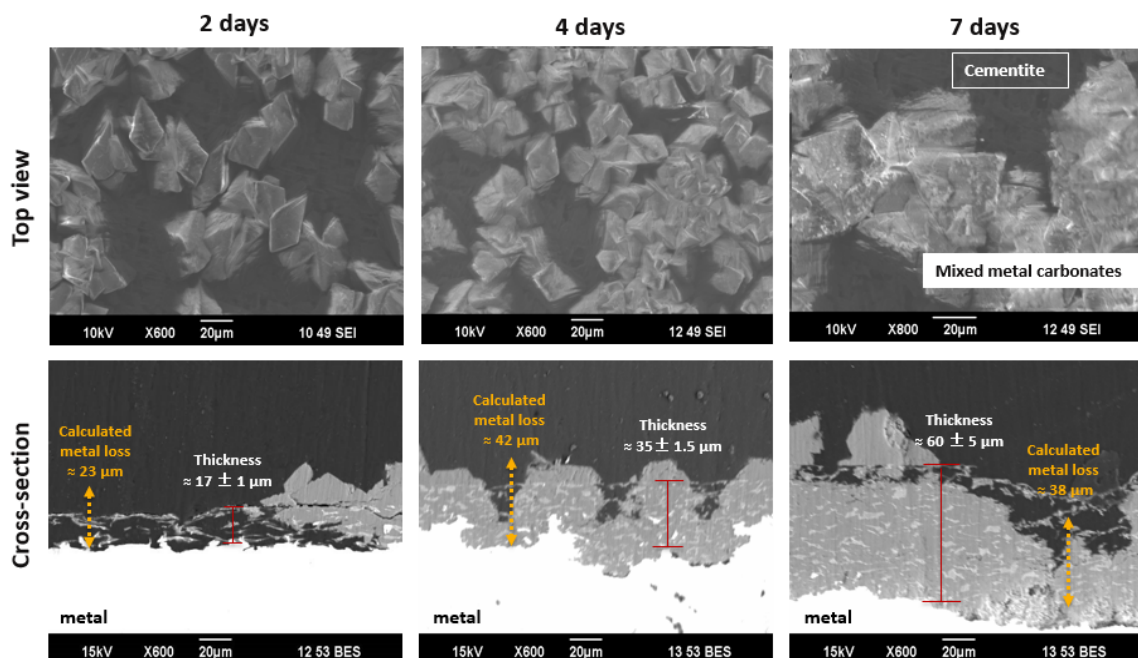


Figure 10. SEM images (top and cross-section view) of the development of surface layers over time for the experiments conducted in the presence of Ca^{2+}

Figure 11 illustrates the chemical composition of the surface layers after 7 days of exposure to the solution saturated with CaCO_3 using the EDS detector. For better data visualization, the graph is divided into 6 zones, from (a) to (f), with different colors. The first zone (a) corresponds to the epoxy resin, used for preparation of specimens for cross-section, with carbon and oxygen being the constituent elements. The line scan enters the cementite structure in the second zone (b), with carbon and iron being the constituent elements. The third zone (c) confirms the formation of a mixed solid solution of $\text{Fe}_x\text{Ca}_y\text{CO}_3$ where the mole fraction of Ca is greater than Fe ($y > x$). Therefore, this compound is named “scale” rather than “corrosion product” since Ca is dominant over Fe. This zone comprises the main portion of surface layers with an approximate thickness of $45 \mu\text{m}$. Zone (d) begins with a critical point where the mole fractions of Ca and Fe are equal within the solid solution of $\text{Fe}_x\text{Ca}_y\text{CO}_3$ ($x=y$). However, closer to the steel surface, the mole fraction of Fe becomes dominant over Ca. Therefore, the surface layer precipitated in this zone is considered a “corrosion product” with the partial incorporation of Ca. Zone (e) is located very close to the steel surface with approximately $12 \mu\text{m}$ thickness. In this zone, Ca is not present and a pure FeCO_3 is formed. Eventually, the line scan enters the steel substrate in zone (f). The presence of carbon in this zone is mainly considered to be due to contamination from epoxy resin that occurs during the polishing process.

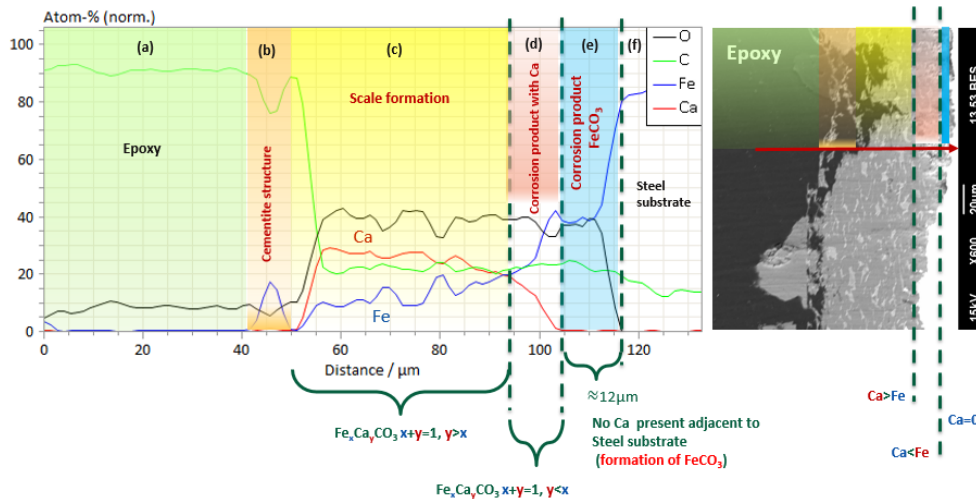


Figure 11. EDS analysis (line scan) of the surface layers formed on carbon steel after 7 days of exposure to the solution in the presence of Ca^{2+}

Morphological analysis of SEM images (Figure 10) and chemical composition characterization of surface layers (Figure 11) suggests the formation of a bilayer on the steel surface in the presence of Ca^{2+} . Very close to the steel surface and within the Fe_3C network, a pure FeCO_3 phase was formed as the inner layer. The outer layer was comprised of a solid solution of $\text{Fe}_x\text{Ca}_y\text{CO}_3$. The mole fraction of Ca was dominant over Fe as this outer layer grew/developed toward the outer border of the Fe_3C network. Figure 12 (EDS mapping) clearly supports the idea about formation of $\text{Fe}_x\text{Ca}_y\text{CO}_3$ within and on top of the Fe_3C network, along with formation of FeCO_3 adjacent to the steel surface.

As mentioned earlier, the change of water chemistry near the steel surface and within the Fe_3C pores was the main driving force for precipitation of the mixed metal carbonate. Figure 13 shows the XRD patterns of the surface layers after 7 days of exposure to the solution saturated with respect to CaCO_3 . Although X-ray penetration power is limited to reaching the layers close to the steel surface, it is able to provide information relevant to the outer side of the surface layers. As can be seen in Figure 13, the detected carbonate peaks in the presence of Ca^{2+} ions are broadened and located between the reference peaks for CaCO_3 and FeCO_3 . This indicates the formation of a heterogeneous solid solution with chemical formula of $\text{Fe}_x\text{Ca}_y\text{CO}_3$. Peaks associated with $\alpha\text{-Fe}$ and Fe_3C are also present in the detected XRD data.

The vulnerability of the specimens to localized corrosion was also evaluated. Profilometry of the specimen surfaces was performed after removing corrosion product layers by Clarke solution²⁸ and no localized corrosion was observed for experiments with or without Ca^{2+} .

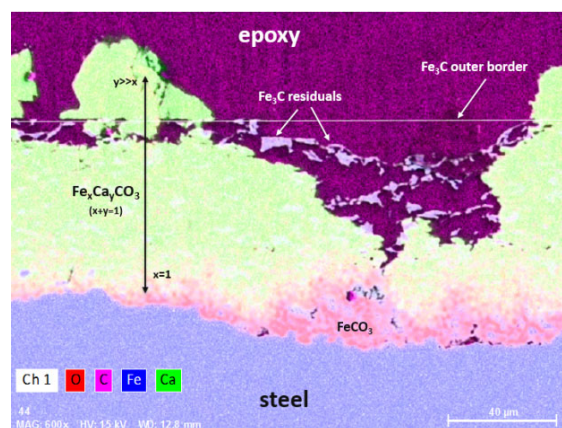


Figure 12. EDS analysis (map mode) confirms formation of corrosion product (FeCO_3) adjacent to the steel surface (inner layer) and a solid solution of $\text{Fe}_x\text{Ca}_y\text{CO}_3$ as the outer layer on the steel after 7 days of exposure to a solution saturated with CaCO_3

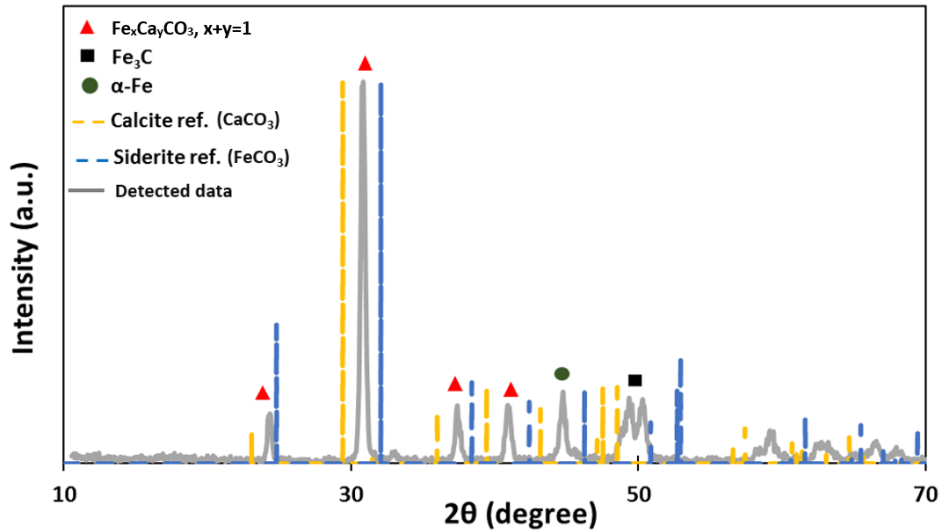


Figure 13. XRD patterns of the surface layers formed on UNS G10180 specimen after 7 days of exposure to a CaCO_3 -saturated solution at 80°C , bulk solution pH 5.5, $p\text{CO}_2$ 0.53 bar, 0.6M ionic strength, and 6000 ppm Ca^{2+}

A Descriptive Model (1st scenario: Mixed iron-calcium carbonate)

Based on the experimental results, a descriptive model is proposed for the mechanism of CO_2 corrosion of mild steel (with ferritic-pearlitic microstructure) exposed to a CaCO_3 -saturated solution with a high concentration of Ca^{2+} at 80°C , bulk solution pH 5.5, $p\text{CO}_2$ 0.53 bar, 0.6M ionic strength:

- (a) UNS G1018 carbon steel is exposed to solution saturated with CaCO_3 and CO_2 as shown in Figure 14a;
- (b) Fe dissolves and Fe^{2+} ions are released into solution. Consequently, a porous Fe_3C network is left behind on the steel surface and grows in thickness over time, as shown in Figure 14b;
- (c) The Fe_3C layer reaches a critical thickness with a water chemistry completely different within its pores ($S_{\text{CaCO}_3} \gg 1$) as compared to the bulk solution ($S_{\text{CaCO}_3} = 1$). This condition favors nucleation and growth of CaCO_3 . However, due to the presence of Fe^{2+} and isostructurality of calcite (CaCO_3) and siderite (FeCO_3), a substitutional carbonate, $\text{Fe}_x\text{Ca}_y\text{CO}_3$ ($x+y=1$), forms within the pores of the Fe_3C network, as shown in Figure 14c;
- (d) At this stage, almost the entire Fe_3C network is filled with $\text{Fe}_x\text{Ca}_y\text{CO}_3$ ($x+y=1$) with $y \gg x$ for the exterior of the surface layer, as shown in Figure 14d;
- (e) Although the corrosion rate decreases upon precipitation and development of $\text{Fe}_x\text{Ca}_y\text{CO}_3$ on the steel surface, undermining corrosion is ongoing and, as a result, the thickness of the surface layer grows over time, as shown in Figure 14e;
- (f) The presence of mixed carbonates on the steel surface hinders mass transfer of Fe^{2+} outward from the steel, therefore, the solubility limit of FeCO_3 is exceeded adjacent to the steel substrate and beneath the mixed carbonate layers. FeCO_3 is supersaturated in such conditions and forms on the steel surface as an inner layer, as shown in Figure 14f. Precipitation of FeCO_3 and its growth at this stage is responsible for further reduction in corrosion rate.

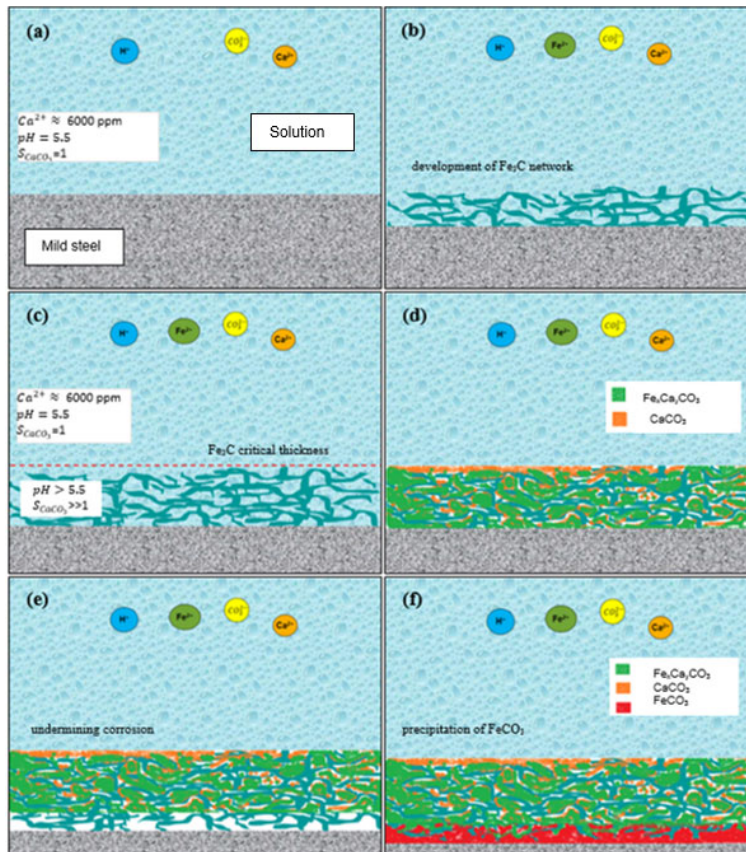


Figure 14. A descriptive model for CO₂ corrosion mechanism of mild steel exposed to the CaCO₃-saturated solution at 80°C, bulk solution pH 5.5, pCO₂ 0.53 bar, 6000 ppm Ca²⁺, and 0.6M ionic strength

Effect of CaCO₃ Scale (2nd scenario: pure CaCO₃)

This section presents the results obtained in the second test series, focusing on determining the protectiveness of pure CaCO₃. There is minimal data in the literature about the protectiveness of CaCO₃ scale (without incorporation of Fe) in CO₂ corrosion of mild steel, as all of the studies are related to situations when FeCO₃ and/or a mixed Fe_xCa_yCO₃ form^{3,16,29,30}. The tests were performed using the same setup as for the previous section and following the conditions summarized in

Table 2. The analysis of the results first focuses on the characteristics of the precipitated CaCO₃ and then addresses its protectiveness against CO₂ corrosion.

Formation of a CaCO₃ Scale

Figure 15 shows the morphology of the surface layer formed on the mild steel surface during 5 days of exposure to the electrolyte and under continuous cathodic polarization. The SEM cross-section image reveals a thin and compact (5-7 μm) layer. The cracks seen in the steel part of the cross-section image are likely generated during the polishing process. The chemical composition analysis by EDS confirmed that such a surface layer is indeed pure CaCO₃ without any incorporation of Fe. Figure 16 and Figure 17 show EDS mapping and line scan analysis of the top and cross-section surface layers, respectively. It is clear that Fe did not incorporate into CaCO₃ during its crystallization and that pure CaCO₃ scale precipitated on the steel surface.

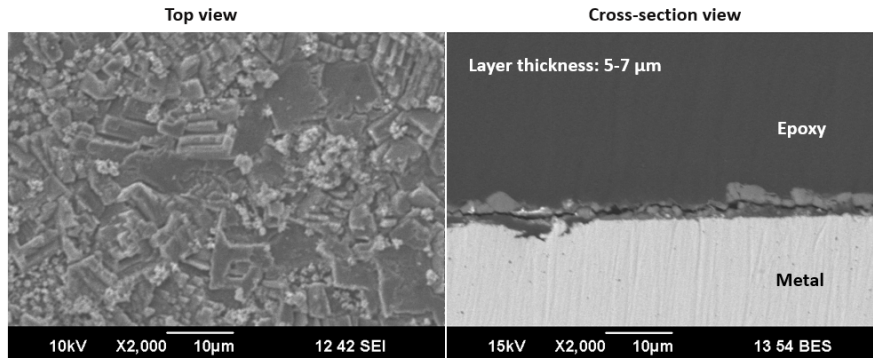


Figure 15. Top and cross-section view SEM of the surface layers formed on the steel during 5 days of cathodic polarization; CaCO_3 -saturated solution, 80°C , bulk solution pH 5.5, $p\text{CO}_2$ 0.53 bar, 6000 ppm Ca^{2+} , and 0.6M ionic strength

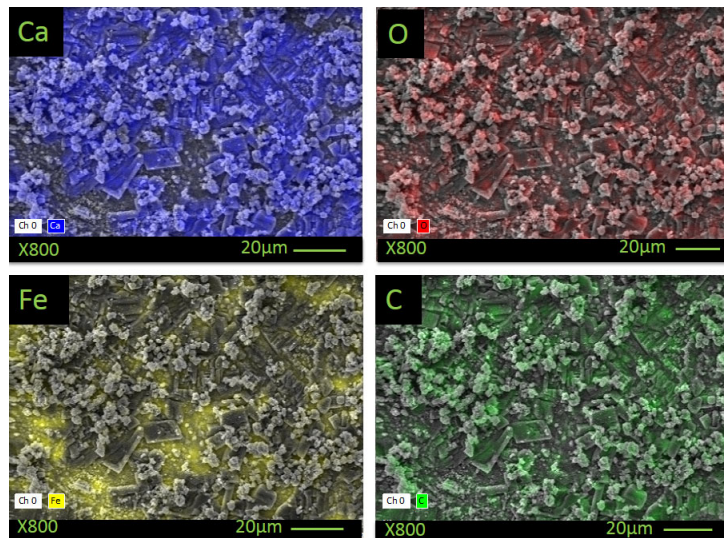


Figure 16. SEM and EDS mapping analysis of the surface layers formed during 5 days of cathodic polarization; Fe is absent in the precipitated crystalline phases.

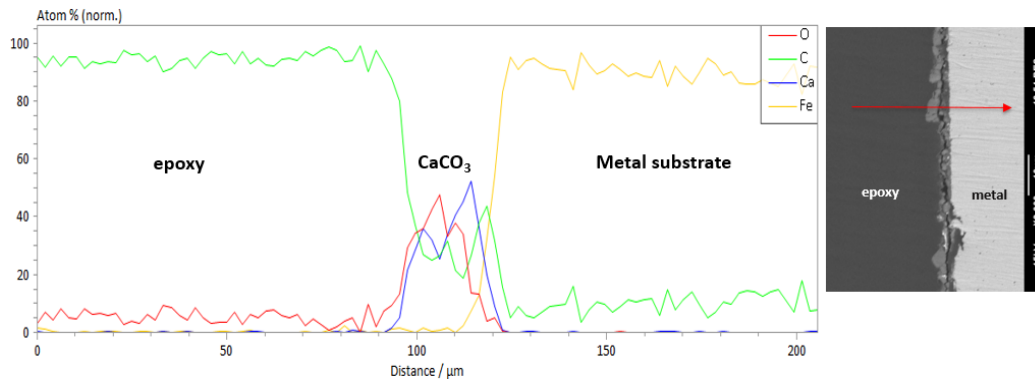


Figure 17. EDS line scan results showing distribution of Ca, C, O, and Fe within the surface layers; formation of CaCO_3 scale.

During the cathodic polarization of the specimens, the corrosion rate was measured once a day at its OCP. To achieve this, the cathodic polarization was briefly halted for about 5 minutes allowing the potential to reach its OCP and then LPR was measured. Figure 18 depicts corrosion rate and potential trends (average OCP and cathodic potential) during the entire duration (5 days) of the experiment. The corrosion rate decreased over time upon precipitation of CaCO_3 scale on the steel surface. From the corrosion rate trend, it could be concluded that CaCO_3 scale can offer some protectiveness against further corrosion. However, this could be a premature conclusion because the metal was also cathodically protected in this period. The average OCP trend over time was almost unchanged and it seemed that formation of CaCO_3 scale did not influence the OCP. One explanation for this observation is that CaCO_3 scale retarded the anodic and cathodic reactions at the same rate by decreasing the active surface area of the steel. As a result, the OCP remained unchanged over time. A question remained whether or not this protectiveness could be retained even after halting of the cathodic polarization. This issue is addressed in the next section.

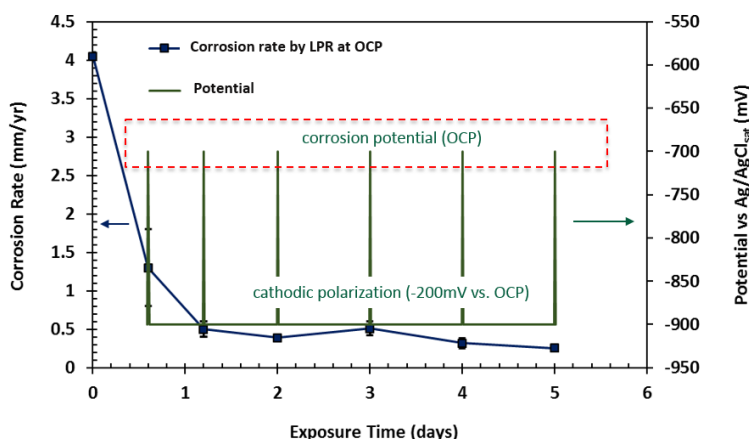


Figure 18. Corrosion rate and potential variations over time during cathodic polarization of the specimens

Halting Cathodic Polarization

After the cathodic polarization was stopped, the CaCO_3 -covered specimen continued to be exposed to the corrosive solution (

Table 2) to investigate the protectiveness of the precipitated scale. Figure 19a and Figure 19b show pH and $[\text{Fe}^{2+}]$ variation over time with and without cathodic polarization. The bulk solution was always saturated with respect to CaCO_3 showing a strong buffering capability toward pH change at the conducted experimental conditions (Figure 19a). As can be seen from Figure 19b, the corrosion rate was well controlled during the polarization period with no measurable Fe^{2+} in the bulk solution. Interestingly, upon removal of the cathodic potential after day 5, Fe^{2+} concentration in the bulk solution increased over the remaining 7 days of the experiment, indicating active corrosion of the steel surface. Figure 20a and Figure 20b compare the corrosion rate obtained with LPR and potential between periods with and without cathodic protection. As can be seen in Figure 20a, in the first 5 days (during cathodic protection), the corrosion rate decreased over time with the formation of CaCO_3 scale. However, after removing the cathodic protection, the corrosion seemed to first increase rapidly, reaching a similar level to that observed at the start of the experiment, and then was observed to decrease over the rest of the experimental duration. The behavior of the second period was more or less similar to the bare steel specimen exposed to the CaCO_3 -saturated solution (first experimental scenario). Figure 20b shows that the OCP was increasing over time after removal of cathodic protection. Such behavior is related to the surface layer development after exposure to the corrosive medium (without cathodic protection).

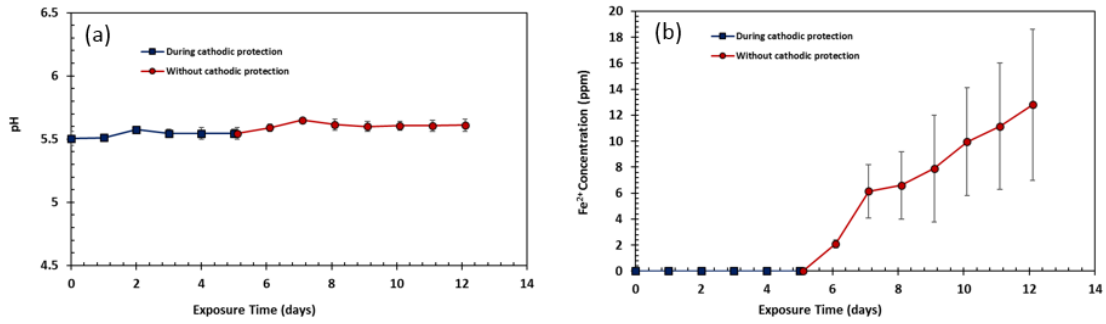


Figure 19. pH (a) and Fe²⁺ concentration (b) variation over time during and without cathodic protection

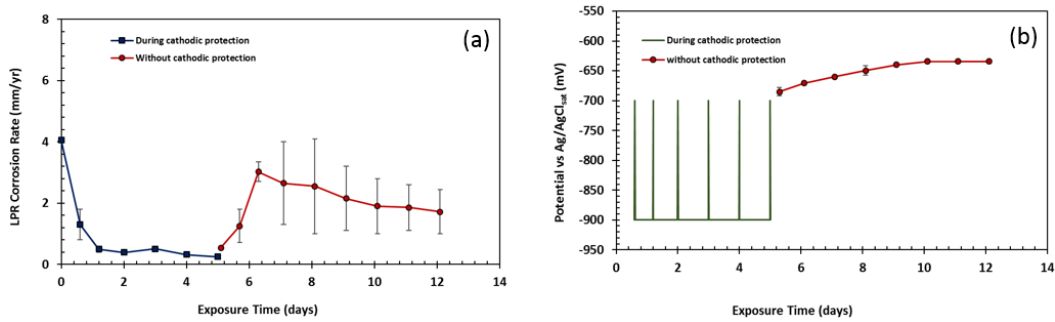


Figure 20. Corrosion rate (a) and potential (b) variation over time during and without cathodic protection

Figure 21 compares the SEM cross-sectional morphology of the specimens obtained with (a) and after removal (b) of the cathodic polarization. The surface layer thickness increased from 5-7 μm at the end of the polarization period to 17-25 μm after 7 days of exposure to the CaCO₃-saturated solution without cathodic polarization. The chemical composition analysis of the layers revealed that the CaCO₃ scale formed during polarization was still present as the outer layer and that a mixed metal carbonate of Fe_xCa_yCO₃ was formed beneath the CaCO₃ layer, driven by corrosion processes as shown in Figure 22. Such analysis confirmed that the corrosion rate decreased upon formation of CaCO₃ scale during polarization (by reducing the anodic and cathodic reactions at the same rate). However, CaCO₃ scale did not maintain its protective behavior when exposed to the corrosive medium without cathodic polarization (active corrosion was observed). Such behavior of CaCO₃ scale was also reported by Ghanbari, *et al.*, in AC corrosion¹⁷. It is noteworthy that despite CaCO₃ (scale) sharing a similar crystal structure to FeCO₃ (corrosion product), CaCO₃ did not show sustained protective behavior against further corrosion while FeCO₃ is widely considered as a potentially protective layer. The main argument is that the constituent cations of CaCO₃ scale and FeCO₃ have different sources. Ca²⁺ ions come from bulk solution while Fe²⁺ ions come from the corroding steel surface. Therefore, FeCO₃ has superior adherence to steel³¹. This is what makes FeCO₃ a potential protective layer in comparison with CaCO₃.

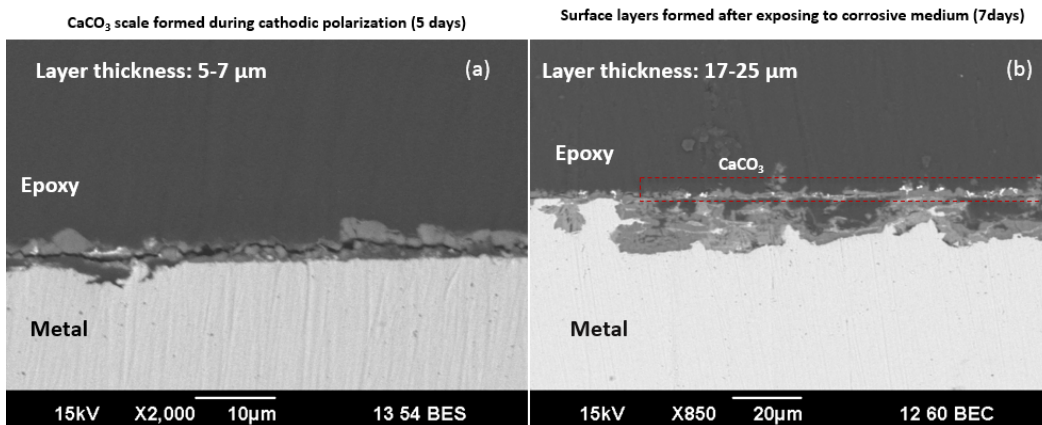


Figure 21. Comparison of surface layer morphologies and thicknesses at the end of the polarization period (5 days exposure) and after exposure to the corrosive medium without cathodic protection (7 days exposure)

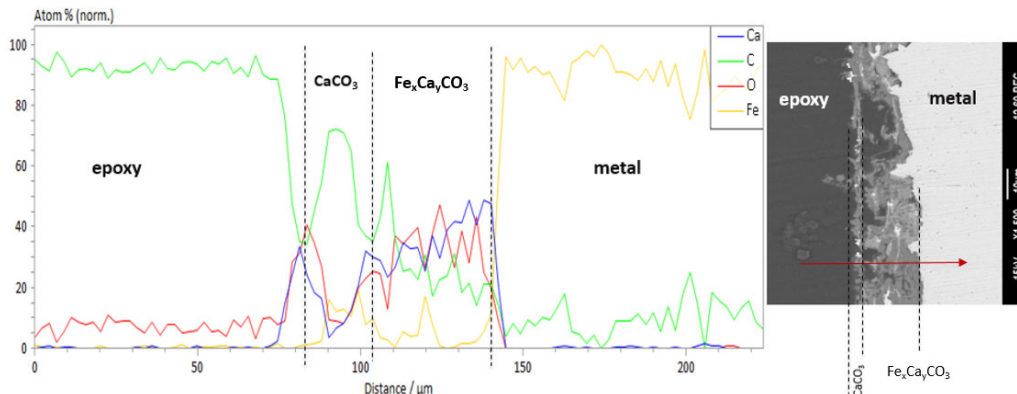


Figure 22. Chemical composition of the layers at the steel surface after 7 days of exposure to a CaCO_3 -saturated solution without cathodic protection of the test specimen

SUMMARY OF CORROSION MECHANISMS

Figure 23 compiles the results already presented for the two experiments described above and compares the corrosion rate trend over time of carbon steel considering two different starting conditions: a bare specimen and of a specimen pre-scaled with CaCO_3 . The two specimens were exposed to the same experimental conditions illustrated in Table 1, and no cathodic polarization was applied at that point. The purpose of this comparison is to investigate if the presence of CaCO_3 has any effect on the corrosion trend and on the steady state corrosion rate. The bare specimen showed a higher initial corrosion rate over the first days of the experiment compared to the pre-scaled specimens. However, the final corrosion rate of both specimens was identical at the end of the experiments. It can be concluded that CaCO_3 scale is not protective in the conducted experimental conditions. However, its presence accelerated the formation of $\text{Fe}_x\text{Ca}_y\text{CO}_3$ and/or FeCO_3 by hindering mass transfer of Fe^{2+} from the steel surface to the bulk solution. For the bare specimen, the development of Fe_3C was also a mass transfer barrier for Fe^{2+} , however, the galvanic effect between Fe_3C and $\alpha\text{-Fe}$ phases led to a pronounced acceleration of the corrosion rate, as compared to the pre-scaled specimens in the active corrosion zone.

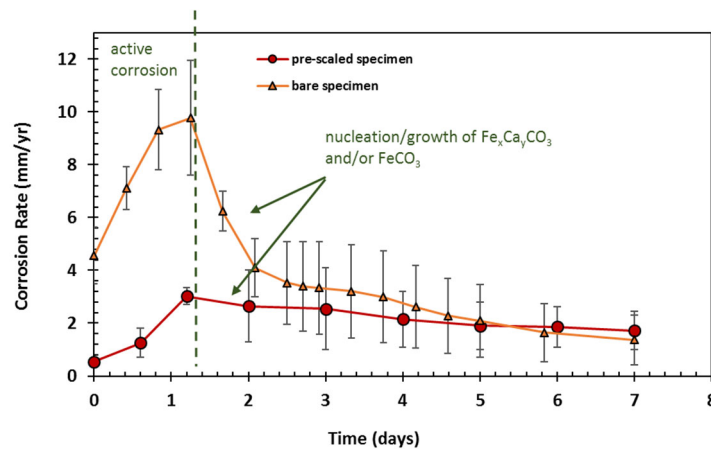


Figure 23. Comparison of corrosion behavior of mild steel with and without CaCO_3 scale at the same experimental condition

CONCLUSIONS

The protectiveness of pure CaCO_3 and mixed $\text{Fe}_x\text{Ca}_y\text{CO}_3$ scale ($x+y=1$ and $y>x$) was investigated in CaCO_3 -saturated solutions in the presence of high concentrations of Ca^{2+} . At the conducted experimental conditions ($S_{\text{CaCO}_3} = 1$, 80°C , bulk solution pH 5.5, $p\text{CO}_2$ 0.53 bar, 0.6M ionic strength, and ~6000 ppm Ca^{2+}), the following conclusions can be made:

- CaCO_3 and $\text{Fe}_x\text{Ca}_y\text{CO}_3$ scale ($x+y=1$ and $y>x$) acted as a mass transfer barrier and promoted surface conditions favoring FeCO_3 precipitation. The final reduction of corrosion rate was attributed to formation of FeCO_3 adjacent to the steel surface.
- CaCO_3 scale by itself was not protective against further corrosion. Although CaCO_3 is isomorphous with FeCO_3 , Ca^{2+} ions come from bulk solution while Fe^{2+} ions come from the corroding steel surface. The growth of FeCO_3 occurs immediately on the steel surface, as Fe^{2+} is released due to corrosion and consumed by crystal growth. Therefore, FeCO_3 has superior adherence to the steel and offers protection against corrosion while CaCO_3 does not.
- Precipitation of CaCO_3 and $\text{Fe}_x\text{Ca}_y\text{CO}_3$ scale ($x+y=1$ and $y>x$) was not observed to promote localized corrosion.

ACKNOWLEDGEMENTS

The author also would like to thank the following companies for their financial support: Anadarko, Baker Hughes, BP, Chevron, CNOOC, ConocoPhillips, DNV GL, ExxonMobil, M-I SWACO (Schlumberger), Multi-Chem (Halliburton), Occidental Oil Company, PTT, Saudi Aramco, SINOPEC (China Petroleum), and TOTAL.

REFERENCES

- [1] Z. D. Cui, S. L. Wu, S. L. Zhu, and X. J. Yang, "Study on corrosion properties of pipelines in simulated produced water saturated with supercritical CO_2 ," *Appl. Surf. Sci.*, vol. 252, no. 6, pp. 2368–2374, Jan. 2006.
- [2] C. de Waard, U. Lotz, and D. E. Milliams, "Predictive Model for CO_2 Corrosion Engineering in Wet Natural Gas Pipelines," *Corrosion*, vol. 47, no. 12, pp. 976–985, Dec. 1991.
- [3] K. Gao *et al.*, "Mechanical Properties of CO_2 Corrosion Product Scales and Their Relationship to Corrosion Rates," *Corros. Sci.*, vol. 50, no. 10, pp. 2796–2803, Oct. 2008.
- [4] J. Han, J. W. Carey, and J. Zhang, "Effect of sodium chloride on corrosion of mild steel in CO_2 -saturated brines," *J. Appl. Electrochem.*, vol. 41, no. 6, pp. 741–749, Jun. 2011.
- [5] B. R. Linter and G. T. Burstein, "Reactions of pipeline steels in carbon dioxide solutions," *Corros. Sci.*, vol. 41, no. 1, pp. 117–139, Jan. 1999.
- [6] Z. Belarbi, B. George, N. Moradighadi, D. Young, S. Nestic, and M. Singer, "Volatile Corrosion Inhibitor for Prevention of Black Powder in Sales Gas Pipelines," in *NACE*, 2018.
- [7] P. E. Dresel and A. W. Rose, "Chemistry and Origin of Oil and Gas Well Brines in Western Pennsylvania," The Pennsylvania State University, Open-File Report OFOG 10–01.0, 2010.
- [8] H. Mansoori, R. Mirzaee, F. Esmailzadeh, A. Vojood, and A. Soltan Dowrani, "Pitting Corrosion Failure Analysis of a Wet Gas Pipeline," *Eng. Fail. Anal.*, vol. 82, pp. 16–25, Dec. 2017.
- [9] A. Rashedi, "A Study of Surface Wetting in Oil-Water Flow in Inclined Pipeline," Master Thesis, Ohio University, 2016.

- [10] H. Mansoori and R. Mirzaee, "On the Predictability of CO₂ Pitting Corrosion in Multiphase Gas Pipelines-An Upstream Case Study," presented at the NACE, 2018.
- [11] H. Mansoori, D. Young, B. Brown, and M. Singer, "Influence of Calcium and Magnesium Ions on CO₂ Corrosion of Carbon Steel in Oil and Gas Production Systems-A Review," *J. Nat. Gas Sci. Eng.*, 2018.
- [12] S. N. Esmaeely, Y.-S. Choi, D. Young, and S. Netic, "Effect of Calcium on the Formation and Protectiveness of Iron Carbonate Layer in CO₂ Corrosion," *Corrosion*, vol. 69, no. 9, pp. 912–920, May 2013.
- [13] Y. Hua, A. Shamsa, R. Barker, and A. Neville, "Protectiveness, morphology and composition of corrosion products formed on carbon steel in the presence of Cl⁻, Ca²⁺ and Mg²⁺ in high pressure CO₂ environments," *Appl. Surf. Sci.*, vol. 455, pp. 667–682, Oct. 2018.
- [14] S. N. Esmaeely, D. Young, B. Brown, and S. Netic, "Effect of Incorporation of Calcium into Iron Carbonate Protective Layers in CO₂ Corrosion of Mild Steel," *Corrosion*, vol. 73, no. 3, pp. 238–246, Nov. 2016.
- [15] L. M. Tavares, E. M. da Costa, J. J. de O. Andrade, R. Hubler, and B. Huet, "Effect of Calcium Carbonate on Low Carbon Steel Corrosion Behavior in Saline CO₂ High Pressure Environments," *Appl. Surf. Sci.*, vol. 359, pp. 143–152, Dec. 2015.
- [16] H. Mansoori, D. Young, B. Brown, and S. Netic, "Effect of CaCO₃-Saturated Solution on CO₂ Corrosion of Mild Steel Explored in a System with Controlled Water Chemistry and Well Defined Mass Transfer Conditions," *Corrosion Science*, 2019.
- [17] E. Ghanbari and R. S. Lillard, "The Influence of CaCO₃ Scale Formation on AC Corrosion Rates of Pipeline Steel Under Cathodic Protection," *Corrosion*, vol. 74, no. 5, pp. 551–565, 2017.
- [18] W. B. Fortune and M. G. Mellon, "Determination of iron with o-phenanthroline: a spectrophotometric study," *Ind. Eng. Chem. Anal. Ed.*, vol. 10, no. 2, pp. 60–64, 1938.
- [19] Z. Duan and D. Li, "Coupled phase and aqueous species equilibrium of the H₂O–CO₂–NaCl–CaCO₂ system from 0 to 250 °C, 1 to 1000 bar with NaCl concentrations up to saturation of halite," *Geochim. Cosmochim. Acta*, vol. 72, no. 20, pp. 5128–5145, Oct. 2008.
- [20] S. Netic, "Key Issues Related to Modelling of Internal Corrosion of Oil and Gas Pipelines – A Review," *Corros. Sci.*, vol. 49, no. 12, pp. 4308–4338, Dec. 2007.
- [21] M. Nordsveen, S. Netic, R. Nyborg, and A. Stangeland, "A Mechanistic Model for Carbon Dioxide Corrosion of Mild Steel in the Presence of Protective Iron Carbonate Films—Part 1: Theory and Verification," *Corrosion*, vol. 59, no. 5, pp. 443–456, May 2003.
- [22] W. Sun, S. Netic, and R. C. Woollam, "The Effect of Temperature and Ionic Strength on Iron Carbonate (FeCO₃) Solubility Limit," *Corros. Sci.*, vol. 51, no. 6, pp. 1273–1276, 2009.
- [23] J. Han, S. Netic, Y. Yang, and B. Brown, "Spontaneous passivation observations during scale formation on mild steel in CO₂ brines," *Electrochimica Acta*, vol. 56, no. 15, pp. 5396–5404, Jun. 2011.
- [24] F. Farelas, B. Brown, S. Netic, and others, "Iron carbide and its influence on the formation of protective iron carbonate in CO₂ corrosion of mild steel," in *NACE*, 2013.
- [25] J. L. Crolet, N. Thevenot, and S. Netic, "Role of conductive corrosion products in the protectiveness of corrosion layers," *Corrosion*, vol. 54, no. 3, pp. 194–203, 1998.

- [26] C. A. Palacios and J. R. Shadley, "Characteristics of corrosion scales on steels in a CO₂-saturated NaCl brine," *Corrosion*, vol. 47, no. 2, pp. 122–127, 1991.
- [27] S. Ieamsupapong, "Mechanisms of Iron Carbonate Formation on Mild Steel in Controlled Water Chemistry Conditions," PhD Dissertation, Ohio University, 2016.
- [28] ASTM G1 (2011), "Standard Practice for Preparing, Cleaning, and Evaluating Corrosion Test." ASTM, 2011.
- [29] C. Ding, K. Gao, and C. Chen, "Effect of Ca²⁺ on CO₂ Corrosion Properties of X65 Pipeline Steel," *Int. J. Miner. Metall. Mater.*, vol. 16, no. 6, pp. 661–666, Dec. 2009.
- [30] Q. Xu, K. Gao, Y. Wang, and X. Pang, "Characterization of corrosion products formed on different surfaces of steel exposed to simulated groundwater solution," *Appl. Surf. Sci.*, vol. 345, pp. 10–17, 2015.
- [31] C. Prieto Nieto, E. Anyanwu, D. Young, and M. Singer, "Mechanical Characterization and Adherence of Iron Carbonate on an X65 Steel," presented at the NACE, 2019.